*Progress In Electromagnetics Research, PIER 100, 265–284, 2010*

# ANALYSIS OF VITAL SIGNS MONITORING USING AN IR-UWB RADAR

**A. Lazaro, D. Girbau, and R. Villarino**

Department of Electronic, Electric and Automatic Engineering
Universitat Rovira i Virgili (URV)
Av. Països Catalans 26, Campus Sescelades, Tarragona 43007, Spain

**Abstract**—Ultra-wide Band (UWB) technology is a new, useful and safe technology in the field of wireless body networks. This paper focuses on the feasibility of estimating vital signs — specifically breathing rate and heartbeat frequency — from the spectrum of recorded waveforms, using an impulse-radio (IR) UWB radar. To this end, an analytical model is developed to perform and interpret the spectral analysis. Both the harmonics and the intermodulation between respiration and heart signals are addressed. Simulations have been performed to demonstrate how they affect the detection of vital signs and also to analyze the influence of the pulse waveform. A filter to cancel out breathing harmonics is also proposed to improve heart rate detection. The results of the experiments are presented under different scenarios which demonstrate the accuracy of the proposed technique for determining respiration and heartbeat rates. It has been shown that an IR-UWB radar can meet the requirements of typical biomedical applications such as non-invasive heart and respiration rate monitoring.

## 1. INTRODUCTION

Ultra-wide band (UWB) is a technology that has distinct features because of its extremely wide bandwidth. UWB wireless systems are generally based on the transmission and reception of sub-nanosecond pulses without carriers or modulated short pulses with carriers. It is claimed that such wireless systems can provide low system complexity, low cost, low power consumption and a high data rate [1–5].

There are also many advantages of using UWB for biomedical applications because it radiates and consumes little power, coexists well

Corresponding author: A. Lazaro (antonioramon.lazaro@urv.cat).

with other instruments, and is robust to interference and multipath. The aim of this study is to use wireless sensing devices based on UWB technology to detect vital signs for health care, emergency rescue, and security. Impulse Radio (IR) is a type of UWB signalling which uses very short baseband pulses, typically in the order of a nanosecond, which has also been proposed in health applications such as the ones presented in [6–9]. UWB monitoring of respiration and heart rate has been studied in [7, 9–13]. An alternative for the non-invasive detection of vital signs is microwave Doppler radar [14]. However, Doppler radar techniques present two problems: 1) The difficulty they have in penetrating material and 2) the null point problem [15]. On the other hand, one of the main advantages of the UWB signal is that it can be propagated through objects, so through-the-wall measurements can be made [11, 14, 16, 17]. This feature is especially important in rescue applications.

In this paper, the breathing rate and heartbeat frequency are estimated using an IR-UWB Radar. Typically, in relaxed human beings the heart can cause chest displacements of 0.08 mm, and respiration displacements of between 0.1 mm and several millimeters, depending on the person [18]. As theoretical formulation and experimental results will show below, the spectrum of the detected signal contains several harmonics of the breathing signal that can be much stronger than the frequency component of the heartbeat. These harmonics can be a serious problem if their frequency is close to that of the heart frequency that is to be estimated. Although the breathing signal has been studied in [12], no studies of breath and heart harmonics have been reported in the literature. Since real systems use approximations to ideal Gaussian pulses, it is shown that the pulse waveform has a considerable influence on the breath harmonic level. This influence is studied here. Finally, a simple canceller filter is proposed to suppress breath harmonics in order to better detect the weak fundamental heart frequency.

The paper is organized as follows. Section 2 presents and discusses the proposed measurement setup. The mathematical formulation of the problem is described in Section 3. The signal processing techniques used to estimate the respiration and heart rates are presented in Section 4. Results from real-time measurements are presented and discussed in Section 5. Concluding remarks are given in Section 6.

## 2. MEASUREMENT SETUP

The UWB remote measurement setup is shown in Figure 1. Two UWB antennas, one for transmission and the other for reception, are pointed

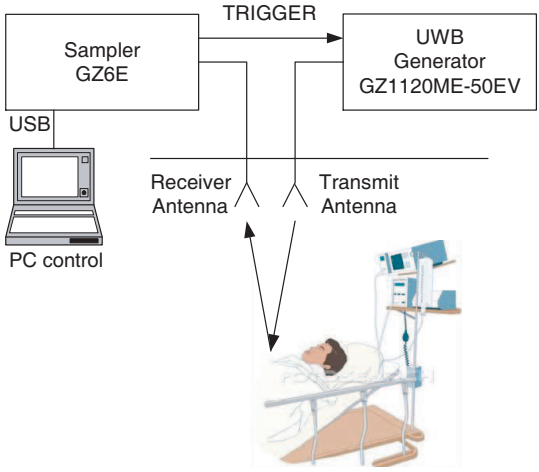


**Figure 1.** UWB-radar test setup.

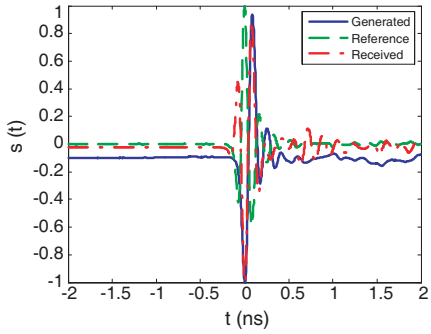


**Figure 2.** Normalized time waveform. Generated (-), received (-.), and reference (- -) obtained from differentiation of the pulse generator waveform.

directly towards the subject. The GZ1120ME-50EV pulse generator (Geozondas) is used to generate a monocycle pulse with a central frequency of 5 GHz, an amplitude of ±5 V and a pulse repetition rate (PRI) of 250 kHz. It is connected to the UWB transmitter antenna (3.1–10.6 GHz frequency range). The radiated pulse is reflected by the person and detected by the receiver antenna. Sampling is done with the GZ6E sampler converter (Geozondas), which triggers the pulse generator. Figure 2 shows the transmitted, the differentiated transmitted and the received pulse waveforms. Figure 3 shows a comparison between the FCC masks [3] for indoor and outdoor UWB

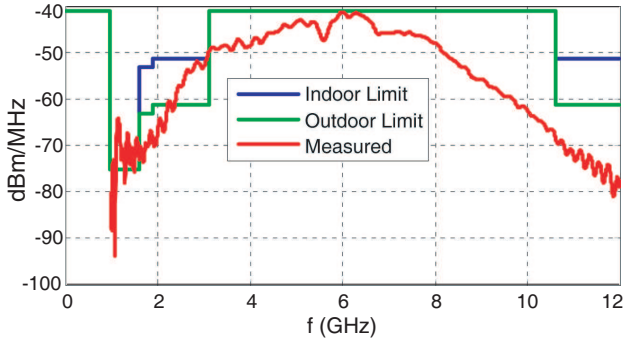


**Figure 3.** Emission mask of UWB radar for medical imaging. Power density measured from Fourier transform of received signal. The FCC indoor and outdoor limits are also shown.

emissions and the power density measured from the Fourier transform of the received signal, after the output power level had been adjusted (except in the mobile wireless frequency bands because of interference in the measurements). The fidelity between the received pulse and the ideal differentiated transmitted pulse is about 90%.

In the experimental results, 64 waveforms are acquired, sampled and averaged to improve the signal-to-noise ratio. The averaged waveform is stored and time gated to avoid antenna coupling signals. The waveforms are sampled using 512 points and the recorded duration is 2.5 ns (although this can depend on the distance between the sampler and the subject). The time-axis associated to range along each received waveform ($\tau$) is usually addressed as "fast-time", and is in the order of nanoseconds. The interval between successive received waveforms is $T_s = 0.0371\,\mathrm{s}$. The time-axis along the measurement interval ($t$) is usually addressed as "slow-time", and is in the order of seconds. This means that the sampling frequency in slow-time, $F_s = 1/T_s = 26.93\,\mathrm{Hz}$, is greater than the Nyquist sampling rate for the heart (signal bandwidth $< 3\,\mathrm{Hz}$) and respiration signals (signal bandwidth $< 0.7\,\mathrm{Hz}$). The measurement interval $T$ is typically chosen to be about 35 s.

## 3. MATHEMATICAL MODEL

One of the goals is to estimate the breathing rate and heartbeat frequency. For this purpose, a mathematical model is developed so that the spectrum of the detected signal can be obtained and understood. This model is an extension of the one proposed in [12] and its main

novelty is that it includes not only breathing but also heart motion. This permits a deep analysis of both harmonics and cross products (intermodulation). The sections below demonstrate that it is very important to make this complete analysis, since the large amplitude of breath harmonics and sometimes of cross products make heart rate measurement a challenge, especially when they are close to the heart frequency range.

When the transmitted pulse hits the human target, part of it is reflected due to the high reflectivity of the body [6, 8]. The time-of-flight or arrival (ToA) of this pulse is denoted by $\tau_0$, and depends on the antenna distance, $d_0$. Due to respiration and heart motion, the chest cavity expands and contracts periodically, so the distance travelled, $d(t)$, varies periodically around the nominal distance $d_0$. For vital signs monitoring, the body movement caused by both respiration and heartbeat must be detected:

$$d(t) = d_0 + m(t) = d_0 + m_b \sin(2\pi f_b t) + m_h \sin(2\pi f_h t) \tag{1}$$

where $m_b$ and $m_h$ are the respiration and heartbeat displacement amplitudes, and $f_b$ and $f_h$ are the respiration and heartbeat frequencies, respectively.

In this situation, the received signal can be represented as the sum of the responses of the channel, and the variation due to the respiration and heartbeat:

$$r(t,\tau) = \sum_i A_i p(\tau - \tau_i) + Ap(\tau - \tau_d(t)) \tag{2}$$

where $p(t)$ is the normalized received pulse, $A_i$ is the amplitude of each multipath component, $\tau_i$ its delay, and $A$ is the amplitude of the pulse reflected on the body. From (2) it is evident that respiration and heart movements modulate the received signal. The time delay $\tau_d$ associated with the vital sign is modeled as the sum of the time-of-flight $\tau_0$ plus two sinusoidal delays associated to respiration and heartbeat displacements:

$$\tau_d(t) = 2d(t)/c = \tau_0 + \tau_b \sin(2\pi f_b t) + \tau_h \sin(2\pi f_h t) \tag{3}$$

where $c$ is the light velocity, and $\tau_b$ and $\tau_h$ are the respiration and heartbeat displacements, respectively.

The received waveforms are measured at discrete instants in slow time $t = nT_s$ $(n = 1, 2 \ldots, N)$. $N$ discrete-time sequences are stored after the received signal is sampled and these values are stored in a matrix $\mathbf{R}$, the elements of which are:

$$R[n,m] = r(\tau = nT_f,\, t = mT_s) \tag{4}$$

where $T_f$ is the sampling period in fast-time.

In a static environment, the resulting clutter can be considered as a DC-component in the slow-time direction. In consequence, the only movement is caused by the person's respiration and heart activity, from (2) it is clear that background clutter does not depend on slow-time $t$. Thus, the background clutter can be removed by filtering the signal. This can be done by subtracting the average of all received waveforms from the original signal (a new matrix $\mathbf{X}$ can be obtained by subtracting the average of all the rows in $\mathbf{R}$ from each row).

$$x(t,\tau) = r(t,\tau) - \lim_{T\to\infty} \frac{1}{T} \int_0^T r(t,\tau)dt = Ap\left(\tau - \tau_d(t)\right) - r_0(\tau) \quad (5)$$

The DC component $r_0(\tau)$ is blocked by subtracting the average of all samples in fast-time (the result is saved in a new matrix $\mathbf{Y}$ that is obtained by subtracting the average of all columns in $\mathbf{X}$ from each column). The signal of interest is:

$$y(t,\tau) = x(t,\tau) - x_0(\tau) = Ap(\tau - \tau_d(t)) \quad (6)$$

The goal is to obtain the breathing frequency $f_b$ and heart rate $f_h$. To this end, the Fourier transform is performed in slow-time $Y(f,\tau)$.

$$Y(f,\tau) = \int_{-\infty}^{+\infty} y(t,\tau)e^{-j2\pi ft}dt \quad (7)$$

The Fourier transform in slow-time $Y(f,\tau)$ can be obtained from the 2D Fourier transform of $y(t,\tau)$, $Y(f,\nu)$:

$$Y(f,\tau) = \int_{-\infty}^{+\infty} Y(f,\nu)e^{j2\pi\nu\tau}d\nu \quad (8)$$

The 2D Fourier transform is given by:

$$Y(f,\nu) = \int_{-\infty}^{+\infty}\int_{-\infty}^{+\infty} y(t,\tau)e^{-j2\pi ft}e^{-j2\pi\nu\tau}dtd\tau \quad (9)$$

$$Y(f,\nu) = \int_{-\infty}^{+\infty} AP(\nu)e^{-j2\pi\nu\tau_d(t)}e^{-j2\pi ft}dt$$

$$= AP(\nu)e^{-j2\pi\nu\tau_0}\int_{-\infty}^{+\infty} e^{-j2\pi\nu m_b\sin(2\pi f_b t)}e^{-j2\pi\nu m_h\sin(2\pi f_h t)}e^{-j2\pi ft}dt \quad (10)$$

where $P(\nu)$ is the Fourier transform (in fast-index) of the received pulse. Using the following expansion of a series of Bessel functions:

$$e^{-jz\sin(2\pi f_0 t)} = \sum_{k=-\infty}^{+\infty} J_k(z) e^{-j2\pi k f_0 t} \tag{11}$$

$Y(f,\nu)$ can be expressed as:

$$\begin{aligned} Y(f,\nu) \;=\; & AP(\nu)e^{-j2\pi\nu\tau_0} \int_{-\infty}^{+\infty} \left( \sum_{k=-\infty}^{+\infty} J_k(\beta_b\nu) e^{-j2\pi k f_b t} \right) \\ & \cdot \left( \sum_{l=-\infty}^{+\infty} J_l(\beta_h\nu) e^{-j2\pi l f_h t} \right) e^{-j2\pi f t} dt \end{aligned} \tag{12}$$

where $\beta_b = 2\pi m_b$ and $\beta_h = 2\pi m_h$. Replacing (12) in (8), the spectrum in slow-time is expressed as:

$$Y(f,\tau) = A \sum_{k=-\infty}^{+\infty} \sum_{l=-\infty}^{+\infty} G_{kl}(\tau)\delta\left(f - kf_b - lf_h\right) \tag{13}$$

where the functions $G_{kl}(\tau)$ are given by the integrals:

$$G_{kl}(\tau) = \int_{-\infty}^{+\infty} P(\nu) J_k\left(\beta_b\nu\right) J_l\left(\beta_h\nu\right) e^{j2\pi\nu(\tau-\tau_0)} d\nu \tag{14}$$

It can be proved that $|G_{kl}(\tau)|$ is maximized at $\tau = \tau_0$:

$$C_{kl} \equiv G_{kl}(\tau_0) = \int_{-\infty}^{+\infty} P(\nu) J_k(\beta_b\nu) J_l(\beta_h\nu) d\nu \tag{15}$$

Consequently:

$$Y(f,\tau_0) = A \sum_{k=-\infty}^{+\infty} \sum_{l=-\infty}^{+\infty} C_{kl}\delta\left(f - kf_b - lf_h\right) \tag{16}$$

From (16), it is clear that the spectrum is a discrete function, consisting of a train of delta functions centred at the frequencies of the harmonics of $f_b$, $f_h$ and their intermodulation products. The amplitude of each intermodulation product for a frequency of $f = kf_b + lf_h$ is controlled by the coefficient $C_{kl}$.

The harmonic components of breathing can be obtained for the index $l$=0:

$$C_{k0} = \int_{-\infty}^{+\infty} P(\nu) J_k(\beta_b \nu) J_0(\beta_h \nu) d\nu \approx \int_{-\infty}^{+\infty} P(\nu) J_k(\beta_b \nu) d\nu \tag{17}$$

The approximation is valid when $\beta_b f_c \ll 1$ ($f_c$ is the central frequency of the pulse), so $J_0(\beta_h \nu) \approx 1$. This result coincides with the development given in [12] for the harmonics of breathing. An analogous result can be obtained for the harmonics of the heartbeat:

$$C_{0l} = \int_{-\infty}^{+\infty} P(\nu) J_0(\beta_b \nu) J_l(\beta_h \nu) d\nu \approx \int_{-\infty}^{+\infty} P(\nu) J_l(\beta_h \nu) d\nu \tag{18}$$

The approximation holds when $\beta_h f_c \ll 1$.

Note that the integrals (15) can be numerically calculated, but they can also be expressed as a function of the Hankel transform. Efficient methods for computing these transformations can be found in the literature [19]. Moreover, a coarse evaluation of the integrals (17) can be obtained with the mean value theorem:

$$C_{kl} \approx \Delta f \cdot J_k(\beta_b f_c) J_l(\beta_h f_c) P(f_c) \tag{19}$$

where $\Delta f$ is the pulse bandwidth.

Although the approximation obtained in (19) is coarse, it can be used to make a qualitative interpretation of the spectrum. For typical UWB pulses that comply with the FCC spectral mask, $f_c$ is about 4–6 GHz. In the case of the heartbeat $\beta_h f_c \ll 1$, $J_l(\beta_h f_c)$ is close to zero. Therefore, this term vanishes rapidly when index $l$ increases. However, when breathing is strong ($m_b = 5$ mm), $\beta_b f_c \approx 1$, and $J_k(\beta_b f_c)$ may be important. Thus, $J_k(\beta_b f_c) \gg J_l(\beta_h f_c)$, so the harmonics of the breathing signal may be strong and may mask the components of the heartbeat. To help to understand this, Figure 4 shows the products of the Bessel functions that are involved in the integral (15) for the first, second and third harmonics of the respiration and the heartbeat frequency, when $m_b = 5$ mm and $m_h = 0.08$ mm. For a pulse that complies with the FCC mask (Figure 3) the main contribution to the integral is in the range of frequencies between 3.1 and 10.6 GHz. If the time waveform of the pulse is an odd function, then the even harmonics of respiration frequency are zero. Figure 4 reinforces this interpretation and shows that the heartbeat components are attenuated considerably more than the respiration components.

Typically, the frequency range of the breathing signal is between 0.2 and 0.7 Hz, and the heartbeat frequency is between 0.8 and 3 Hz. As

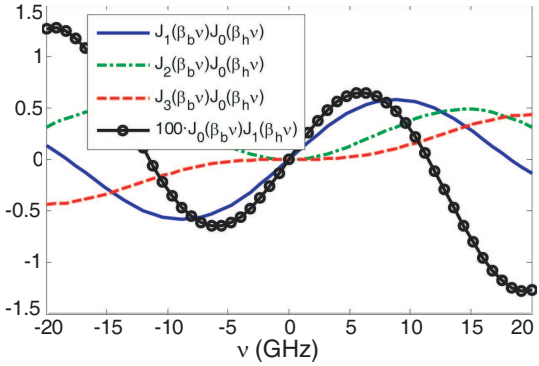


**Figure 4.** Plot of the product of the Bessel functions involved in calculating the Fourier coefficients $C_{10}$, $C_{20}$, $C_{30}$ and $C_{01}$.

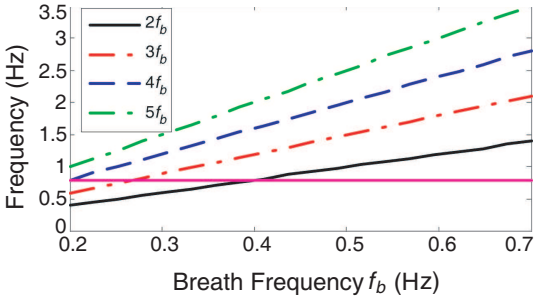


**Figure 5.** Harmonics of breathing ($2f_b$, $3f_b$, $4f_b$, $5f_b$) as a function of breath frequency. The frequencies higher than minimum heartbeat frequency can interfere with heartbeat components ($f_h > 0.8\,\text{Hz}$).

shown in Figure 5, the first harmonics of the breathing signal (and also some intermodulation products) fall within the heartbeat frequency range. As the level of the heartbeat component is very small, it can be difficult to identify. Therefore the heart beat estimation observed from the spectrum peaks can be erroneous Consequently, it is important to evaluate the level of these harmonics and intermodulation components.

In order to investigate the effect of the pulse waveform on the spectrum components, Figure 6 shows the first, second and third harmonics of respiration, the heartbeat component and the intermodulation product at $f = -2f_b + f_h$ as a function of breathing amplitude, for an ideal Gaussian monocycle (first derivative of Gaussian function) with a central frequency of 5 GHz and a heartbeat amplitude $m_h = 0.08\,\text{mm}$. The spectral components were calculated

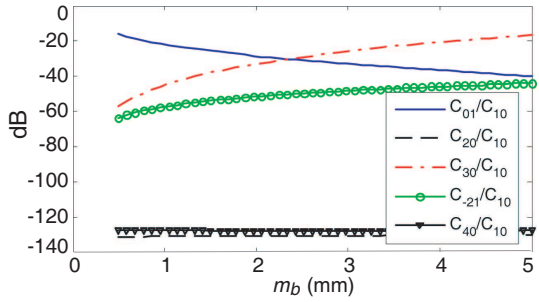


**Figure 6.** Heartbeat component, respiration harmonics ($2f_b$, $3f_b$ and $4f_b$) and intermodulation product ($-2f_b + f_h$) as a function of breath amplitude $m_b$ for a Gaussian monocycle with a central frequency of 5 GHz. Heartbeat amplitude $m_h = 0.08$ mm.

using (15). The results were checked by means of numerical Fourier transform of (6). The Fourier coefficients were normalized with respect to the fundamental breathing component ($C_{10}$). The Gaussian monocycle is an odd function, so the even harmonics ($C_{20}$ and $C_{40}$) of the breathing signal are zero. For this typical value of heartbeat displacement, the level of the heartbeat signal ($C_{01}$) is between 18 and 40 dB below the respiration component. For breathing displacement amplitudes higher than about 2.3 mm, the third harmonic ($C_{30}$) is higher than the heartbeat component ($C_{01}$). This component can prevent the heartbeat frequency from being identified if their frequencies are close. Similar levels were found for other odd order Gaussian pulses ($n = 3$ or 5). The reason is that the pulse spectrum has the same shape if the pulses have the same central frequency and bandwidth. However, the pulse is often not a symmetric function (odd or even function), and some ripples can appear due to antenna distortion. It should also be noted that the amplitude of the third-order intermodulation product ($-2f_b + f_h$) is considerable ($C_{-21}$), especially when the breath amplitude $m_b$ is large, and that its value is comparable to the heart rate amplitude ($C_{01}$). Figure 7 shows the harmonics of the breathing components and intermodulation components for the real pulse received in the experimental setup (Figure 2). The differences between this case and the case of the Gaussian monocycle are considerable. The pulse waveform (Figure 2) is no longer an odd function, so the second respiration harmonic is high (−10 dB with respect to the fundamental breathing component). The third harmonic increases with the breathing amplitude and reaches the same level as the heartbeat component for a breath amplitude $m_b$ of about

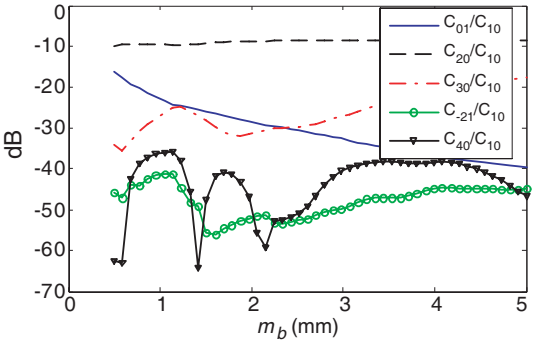


**Figure 7.** Heartbeat component, respiration harmonics ($2f_b$, $3f_b$ and $4f_b$) and intermodulation product ($-2f_b + f_h$) as a function of breath amplitude $m_b$ for the received pulse waveform of Figure 2. Heartbeat amplitude $m_h = 0.08$ mm.

2.4 mm, and the maximum level is about the same value. However, the heartbeat fundamental component ($C_{01}$) has the same levels as for the Gaussian monocycle. It is very important to note that the fourth harmonic and the third-order intermodulation products are comparable to the heartbeat component for high breathing amplitudes. This means that in such situations a complete spectral analysis is essential if the heart rate component is to be correctly detected and confusion with other spectral components avoided. It can be concluded that the pulse's waveform shape does not influence the level of the heartbeat fundamental ($C_{01}$), but it has an important role in the level of the harmonic components of breathing and heartbeat, and also in the level of the intermodulation products.

## 4. HARMONIC CANCELLER

Our study shows that all the harmonics of breathing frequency need to be removed, insofar as this is possible, if the heartbeat frequency is to be detected. To this end, a trap filter is designed. The breathing signal is the highest spectrum component, so the breathing rate can be determined by finding the maximum peak of the Fourier transform of the signal $y(t)$. An alternative to Fast Fourier Transform (FFT) is the Chirp Z-Transform (CZT). The Chirp Z-Transform is a generalization of a Z-Transform that improves the resolution without increasing the number of samples [20]. Since both breath harmonics and intermodulation products are located near the heartbeat component, frequency resolution is an important issue. The ripple in the spectrum

is associated to the time window used and can be reduced with a Hamming window.

The breathing harmonics can be attenuated with a filter based on the Moving Target Indicator (MTI), although it does not separate static clutter from Doppler signals in this case. The basic implementation of a single-delay MTI canceler is shown in Figure 8. The output signal is the difference between the input signal and the same signal delayed one period $T$. In this case, $T$ is the inverse of the breathing rate, $T = 1/f_b$. It is clear that all the harmonic components of the breathing signal are periodic with period $T$, so the output at each frequency is canceled by the filter. To minimize error, a cascade of single-delay filters (such as the one shown in Figure 8) can be used. Although the canceler filter can be implemented using a standard Finite Impulse Response (FIR) filter, we are interested in the output spectrum, which is obtained from the product of the filter transfer function by the spectrum of the input signal. The filter transfer function of a $K$ section filter canceler is given by:

$$H(\omega) = \left(1 - e^{-j\omega T}\right)^K = (2j\sin(\omega T))^K e^{j\omega KT/2} \tag{20}$$

Figure 9 shows the normalized frequency response of a multiple delay canceler as a function of normalized frequency $f \cdot T$. It can be shown that the filter cancels the frequencies that are multiples of $1/T$. Moreover, increasing the order of the canceler, $K$, also increases the canceler bandwidth.

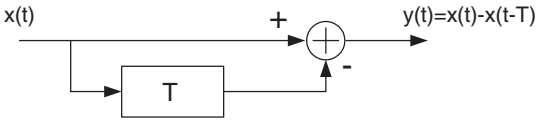


**Figure 8.** Implementation of a single-delay canceller.

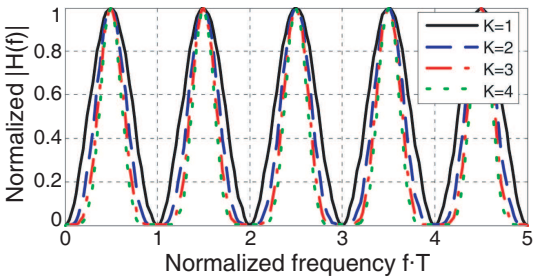


**Figure 9.** Normalized transfer function of a multiple-delay canceller as a function of normalized frequency $f \cdot T$ for order $K = 1, 2, 3, 4$.

## 5. EXPERIMENTAL RESULTS

This section shows some experimental results. Different breathing rates were considered so that the influence of the harmonics of the breathing signal and of intermodulation products could be determined. In the first case, a human target with moderate breathing and heartbeat rates is located 1 m away from the instrument. Figure 10 shows the measured signal as a function of the fast and slow indexes before and after the

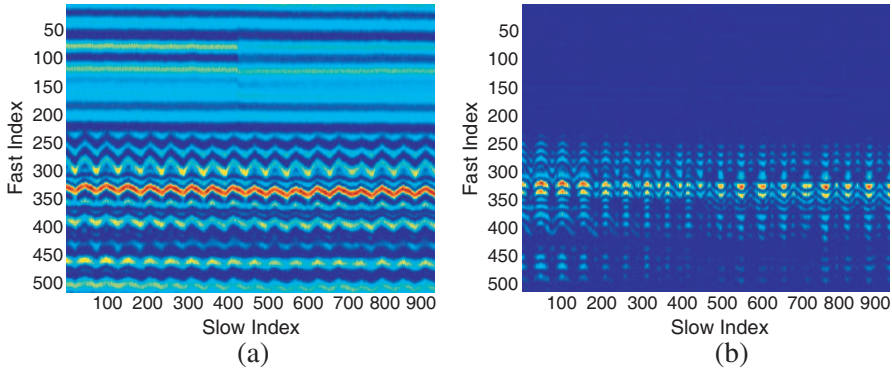


**Figure 10.** Received signal from a man located 1 m away from the radar and after moderate exercise, as a function of fast and slow indexes. (a) Raw data, and (b) signal after clutter removal.

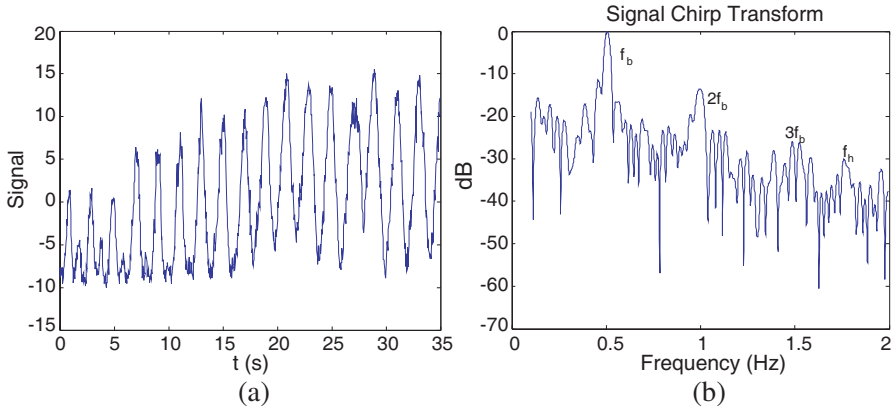


**Figure 11.** (a) Breathing and heart signal in time domain, and (b) its normalized spectrum, for a man located 1 m away from the radar and after moderate exercise.

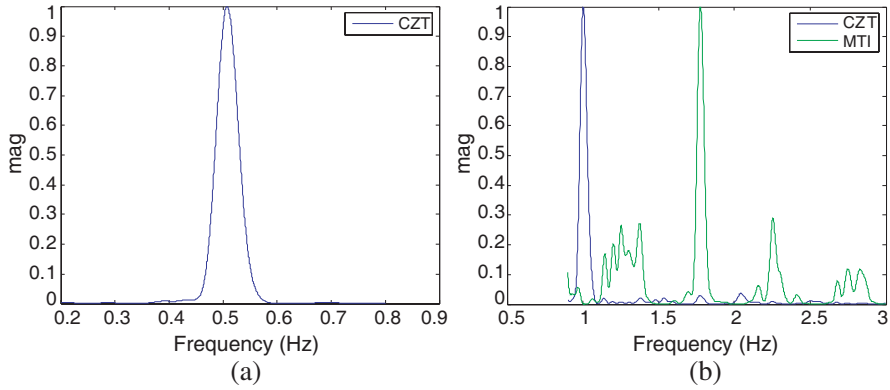


**Figure 12.** (a) Spectrum of the breathing signal in Figure 11, computed using Chirp Z-Transform, and (b) spectrum of the heart signal computed from Chirp Z-Transform before and after the MTI harmonic canceller is applied.

clutter is removed. Figure 11(a) shows the detected signal (which includes breath and heart) in the slow-time domain. The breathing rate is clearly visible; however, the heart signal is masked by harmonics and noise. Figure 11(b) shows the Fourier transform (computed using the Chirp Z-Transform algorithm) of the detected signal, in which the breath harmonics are clearly observed. The breathing rate is detected by finding the maximum peak in the spectrum obtained by means of the Chirp Z-Transform (Figures 11(b) and 12(a)). The estimated value is 0.507 Hz (or 30.46 breath/min). Figure 11(b) shows that the heartbeat signal is 30 dB below the fundamental breathing frequency component. This is in agreement with previous simulations. It is difficult to detect the heart component from the signal in Figure 11(b), since the second and third harmonics are 15 dB and 5 dB higher than the heart level, respectively. However, after the harmonic canceller (MTI canceller) has been applied the heart signal is easily detected. As shown in Figure 12(b), the frequency detected is 1.775 Hz or 106.5 beat/min, and the frequency measured with an electrocardiograph (ECG) is 105 beat/min.

A second case is shown in Figures 13 and 14. The breathing and heartbeat rates are for the same person, located at the same distance (1 meter away from the radar), but in a relaxed situation. The measured heartbeat component is now about 25 dB below the breathing signal. In this case, the third and fourth harmonics of the breathing signal and third order intermodulation products fall in the heart frequency range. As the magnitude of these harmonics is

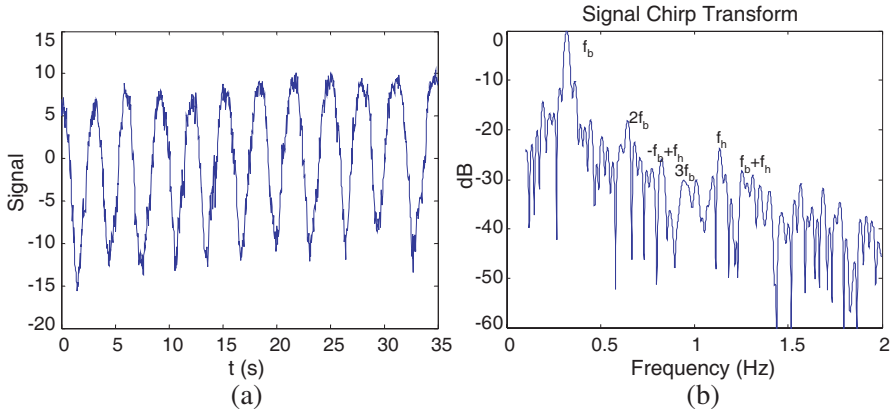


**Figure 13.** (a) Breathing and heart signal in time domain, and (b) its normalized spectrum, for a man located 1 m away from the radar and in repose.

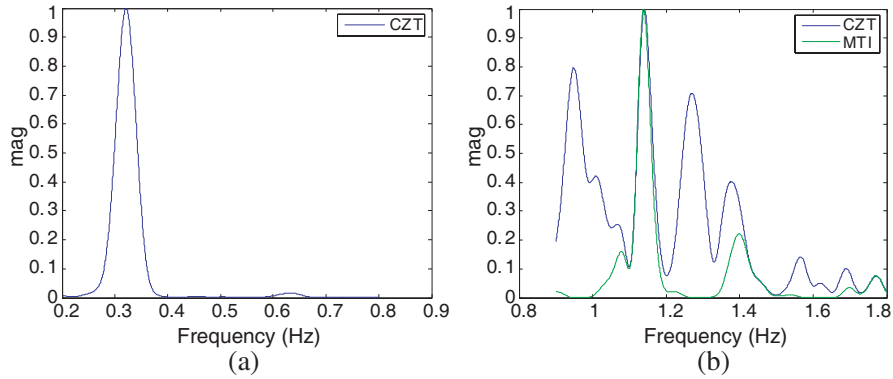


**Figure 14.** (a) Spectrum of the breathing signal in Figure 13 computed using the Chirp Z-Transform, and (b) spectrum of the heart signal computed from Chirp Z-Transform before and after the MTI harmonic canceller has been applied.

smaller than in the previous case, the heart frequency can be found and detected directly; however, the harmonic canceller suppresses the breathing harmonics and intermodulation products, and helps to find and detect the heart rate. Although it is difficult to estimate breathing displacement, the level of the first harmonics shows that it is higher in the first case, after moderate exercise. The breathing frequency detected is 0.32 Hz (19.27 breath/min) and the heart frequency is 1.138 Hz (68.31 beat/min); the heartbeat measured using an ECG is

70 beat/min.

Finally, the third case is a non-line-of-sight (NLOS) case. The same person is located 1 m away from the radar, but now with a brick wall in the middle. The wall is 20 cm thick and has a mean attenuation of 10 dB at the UWB FCC band. As is pointed out in [16, 17], the received pulse is attenuated and distorted after propagation through the wall due to material dispersion. These effects can be modelled as a filter, the transfer function of which can be derived from Fabry-Perot interferometer theory [16, 17]. In addition to the attenuation, which depends on the type of material and the thickness of the wall, the received pulse is no longer symmetrical due to dispersion and the superposition of multiple reflections on the wall. As a result of the pulse distortion, the level of breath harmonics is expected to increase or vary, which can make heart rate detection difficult. Figure 15 shows the raw data and the data after the clutter has been removed. The interesting signal is the second pulse received, since the first one is the direct reflection on the wall. It is independent of breathing, as can be seen in Figure 15(b) where it is practically eliminated even though the reflection on the wall is much more intense than the pulse reflected on the body. Figure 16 shows the detected signal in slow-time and its spectrum. It can be seen that the signal is noisier than in the previous cases due to wall attenuation. The heart signal level is about 20 dB below the breathing signal. Now, the third and fourth harmonics of breath fall in the heart frequency range and are higher than the heart component. Again, after the harmonic canceller has been applied the heart frequency can be determined. In this case, the

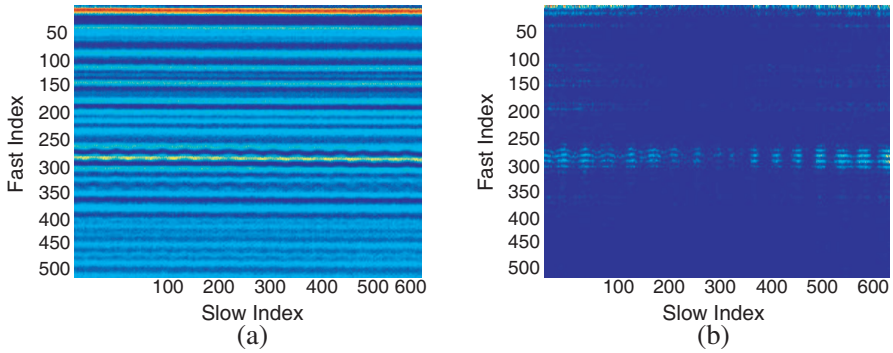


**Figure 15.** Received signal from a man located 1 m away from the radar with a wall in the middle, as a function of fast and slow indexes. (a) Raw data, and (b) signal after clutter removal.

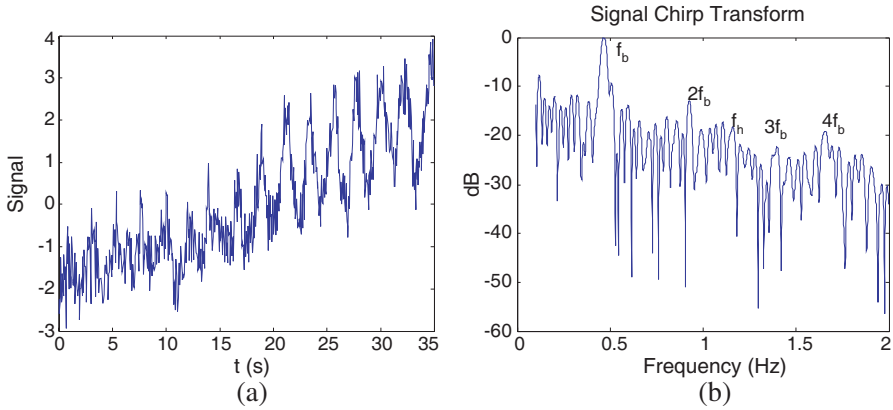


**Figure 16.** (a) Breathing and heart signal in time domain and its normalized spectrum, and (b) for a man located 1 m away from the radar and with a wall in the middle.

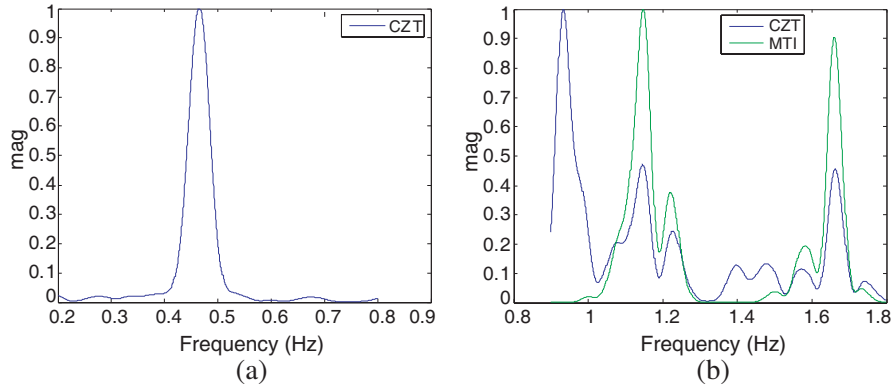


**Figure 17.** (a) Spectrum of the breathing signal in Figure 16 computed using the Chirp Z-Transform, and (b) spectrum of the heart signal computed from the Chirp Z-Transform before and after the MTI harmonic canceller has been applied.

breathing frequency is measured to be 0.465 Hz (27.92 breath/min) and the heartbeat is 1.148 Hz (68.87 beat/min) which is in agreement with the 69 beat/min measured with the ECG.

## 6. CONCLUSION

In this paper, the use of impulse-radio ultra-wide band (IR-UWB) signals in the non-invasive monitoring of breathing and heartbeat rates has been analyzed. A comprehensive analytical study of the spectrum has been made. The breathing rate can be easily estimated from the experimental results presented. However, the level of breath displacement is one order of magnitude larger than heart displacement. In our analysis and experimental observation, estimating the weak heart signal in both the time and frequency domains was hindered not only by noise but also by the harmonics of the breath signal and intermodulation products between breath and heart. As the breath rate and its intensity can depend on the person and the situation, in some cases the frequency of first breath harmonics and/or intermodulation products is close to the frequency of the heart signal, which makes it difficult to locate and detect, leading to possible confusion. It has been theoretically demonstrated that for breath displacements greater than about 2.5 mm, these harmonics have the same magnitude as the heart component. It has also been demonstrated that the shape of the pulse waveform has an important role in harmonic content. This is an important drawback, since the shape of real pulses is far from the shape of an ideal Gaussian monocycle and pulses can be distorted when they cross obstacles such as a wall. On the other hand, it has been shown that the ratio between the fundamental frequency components of breathing and heartbeat is fairly independent of the pulse shape for a given central frequency and bandwidth. To overcome these problems, a harmonic canceller (MTI canceller) has been proposed to automatically remove the harmonics from the breath signal (and, therefore, also to remove intermodulation products).

Experiments have been conducted on a UWB radar prototype operating within an FCC mask (3.1 to 10.6 GHz). Three examples have been described and analyzed: A person after moderate exercise, a person in a relaxed situation and, finally, a person behind a wall. It is concluded that a complete spectrum analysis needs to be made to correctly estimate the usually weak heart signal, which is often hidden by respiration harmonics and third-order intermodulation products. It has been empirically demonstrated that the harmonic canceller and the use of the Chirp Z-Transform help to reliably locate and detect the heartbeat rate, especially when harmonics and intermodulation products fall around the heart frequency range.

## ACKNOWLEDGMENT

This paper was supported by the Spanish Government Project TEC2008-06758-C02-02.

## REFERENCES

1. Zhuang, W., X. Shen, and Q. Bi, "Ultra-wideband wireless communications," *Wirel. Commun. Mob. Comput.*, No. 3, 663–685, 2003.
2. Fontana, R. J., "Recent system applications of short-pulse ultra-wideband (UWB) technology," *IEEE Trans. on Microwave Theory and Tech.*, Vol. 52, No. 9, 2087–2104, 2004.
3. Federal Communications Commission (FCC), "First report and order in the matter of revision of Part 15 of the commission's rules regarding ultra-wideband transmission systems," ET Docket 98–153, FCC 02–48, Apr. 2002.
4. Lu, G., P. Spasojevic, and L. Greenstein, "Antenna and pulse designs for meeting UWB spectrum density requirements," *2003 IEEE Conference on Ultra Wideband Systems and Technologies*, Reston, VA, USA, Nov. 2003,
5. Pozar, D. M., "Waveform optimization for ultrawideband radio systems," *IEEE Trans. Antennas Propag.*, Vol. 31, No. 9, 2335–2345, 2003.
6. Staderini, E. M., "UWB radars in medicine," *IEEE Aerospace and Electronic Systems Magazine*, No. 1, 13–18, 2002.
7. McEwan, T. E., "Body monitoring and imaging apparatus and method," US Patent 5,766,208.
8. Bilich, C. G., "Bio-medical sensing using ultra wideband communications and radar technology: A feasibility study," *IEEE Pervasive Health Conference and Workshops*, 1–9, Nov. 2006.
9. Bond, E. J., L. Xu, S. C. Hagness, and B. D. Van Veen, "Microwave imaging via space-time beamforming for early detection of breast cancer," *IEEE Trans. Ant. Prop.*, Vol. 51, No. 8, 1690–1704, 2003.
10. Ossberger, G., T. Buchegger, E. Schimback, A. Stelzer, and R. Weigel, "Non-invasive respiratory movement detection and monitoring of hidden humans using ultra wideband pulse radar," *Proc. of the 2004 International Workshop on Ultra Wideband Systems Joint with Conference on Ultra Wideband Systems and Technologies*, 395–399, Piscataway, NJ, USA, 2004.
11. Chia, M. Y. W., S. W. Leong, C. K. Sim, and K. M. Chan,

"Through-wall UWB radar operating within FCC's mask for sensing heart beat and breathing rate," *IEEE European Microwave Conf. 2005*, Vol. 3, 1–4, 2005.

12. Venkatesh, S., C. Anderson, N. V. Rivera, and R. M. Buehrer, "Implementation and analysis of respiration-rate estimation using impulse-based UWB," *2005 IEEE Military Communications Conference (IEEE Milcom'05)*, Vol. 5, 3314–3320, Oct. 2005.
13. Immoreev, I. and T.-H. Tao, "UWB radar for patient monitoring," *Aerospace and Electronic Systems Magazine*, No. 11, 11–18, 2008.
14. Ivashov, S. I., V. V. Razevig, A. P. Sheyko, and I. A. Vasilyev, "Detection of human breathing and heartbeat by remote radar," *Progress In Electromagnetic Research Symposium*, 663–666, Pisa, Italy, Mar. 28–31, 2004.
15. Lubecke, O. B., P. W. Ong, and V. M. Lubecke, "10 GHz doppler radar sensing of respiration and heart movement," *2002 IEEE Proceedings of the IEEE 28th Annual Northeast Bioengineering Conference*, 55–56, Apr. 20–21, 2002.
16. Pinhasi, Y., A. Yahalom, and S. Petnev, "Propagation of ultra wide-band signals in lossy dispersive media," *IEEE International Conference on Microwaves, Communications, Antennas and Electronic Systems, COMCAS 2008*, 1–10, May 13–14, 2008.
17. Safaai-Jazi, A., S. M. Riad, A. Muqaubel, and A. Bayram, "Report on through-the-wall propagation and material characterization," DARPA NETEX program "Ultrawideband propagation measurements and channel modeling," Nov. 2002.
18. Singh, M. and G. Ramachandran, "Reconstruction of sequential cardiac in-plane displacement patterns on the chest wall by laser speckle interferometry," *IEEE Trans. Biomed. Eng.*, Vol. 38, No. 5, 483–489, 1991.
19. Siegmann, A. E., "Quasi fast Hankel transform," *Optical Letters*, Vol. 1, 13–15, 1977.
20. Rabiner, L. R., R. W. Schafer, and C. M. Rader, "The Chirp Z-Transform algorithm and its applications," *The Bell System Technical Journal*, 1249–1292, May–Jun. 1969.